This is a preprint, the final version is subject to change, of the American Mineralogist (MSA)
Cite as Authors (Year) Title. American Mineralogist, in press.
(DOI will not work until issue is live.) DOI: http://dx.doi.org/10.2138/am-2016-5586

revision 2

# Experimental investigation of the kinetics of the spinel-to-garnet transformation in peridotite: a preliminary study

Maiko Nagayoshi[1], Tomoaki Kubo[2,*], Takumi Kato[2]

[1]Department of Earth and Planetary Sciences, Graduate school of Science, Kyushu University, Fukuoka 819-0395, Japan

[2]Department of Earth and Planetary Sciences, Faculty of Science, Kyushu University, Fukuoka 819-0395, Japan

*Corresponding author: Tomoaki Kubo

Department of Earth and Planetary Sciences, Faculty of Science, Kyushu University,

Fukuoka 819-0395, Japan

TEL & FAX: +81-92-802-4195

e-mail: kubotomo@geo.kyushu-u.ac.jp

## ABSTRACT

To study the kinetics of the spinel-to-garnet transformation in peridotite, we conducted reaction experiments in the garnet peridotite stability field (3.2 GPa, 1020°C–1220°C, for 0.6–30 hours) using a single spinel crystal embedded in monomineralic orthopyroxene powder or in a mixture of powdered orthopyroxene and clinopyroxene. The growth textures observed in the reaction rim between the spinel crystal and the polycrystalline pyroxenes show that the reaction rim grew in both the spinel and pyroxenes directions, suggesting mobility of both $SiO_2$ and $R_2O_3$ components (where R is a trivalent cation). Olivine grains formed only in the presence of monomineralic orthopyroxene, and were present in some domains without forming reaction rims. Based on a diffusion-controlled growth model, the growth kinetics of the garnet reaction rim can be described by $[x(t)]^2 = k_0 \exp(-H^*/RT)t$, where x(t) is the rim width at time t, R is the gas constant, T is the absolute temperature, and H* is the activation enthalpy of reaction; $k_0$ and H* are, respectively, $k_0 = 10^{-19.8 \pm 4.9}$ $m^2$ $s^{-1}$ and $H^* = 171 \pm 58$ kJ $mol^{-1}$. The development of a garnet reaction rim around a spinel core has been observed in alpine-type peridotitic rocks and mantle xenoliths. The reaction rims experimentally produced in this study are characteristic of corona textures observed in natural rocks, and the experimentally measured growth rate of the rims places important constraints on dynamic transformation processes involving spinel and garnet in peridotite. However, to reconstruct the P–T–t history of the corona texture based on these elementary processes, additional detailed studies on the textural evolution and quantitative kinetics of the garnet-rim growth stage are required.

**Keywords**: spinel; garnet; peridotite; reaction rim growth; kinetics; experimental petrology; UHP metamorphism

## INTRODUCTION

The phase transformation from spinel peridotite to garnet peridotite, occurring in the Earth's upper mantle, involves the reaction of spinel with pyroxenes to form garnet. The existence of pyropic garnet provides important evidence for the deep origin of mantle-derived rocks. This transformation is generally described by the following reaction (e.g., Kushiro and Yoder, 1966):

$$\text{Opx} + \text{Cpx} + \text{Spl} = \text{Grt} + \text{Ol} \quad (1)$$

where Opx, Cpx, Spl, Grt, and Ol represent orthopyroxene, clinopyroxene, spinel, garnet, and olivine, respectively. The phase boundary for this transformation has been experimentally determined in the $CaO–MgO–Al_2O_3–SiO_2$ (CMAS) system (e.g., Kushiro and Yoder, 1966; O'Hara et al., 1971; Milholland and Presnall, 1998; Klemme and O'Neill 2000; Walter et al., 2002) and in natural peridotite (e.g., O'Hara et al., 1971). The boundary, which has a positive Clapeyron slope, is located at ~1.7–2.0 GPa and ~1000°C–1200°C, corresponding to a depth of ~60 km (Fig. 1). It has been suggested that the Clapeyron slope becomes negative at temperatures below ~800°C, based on thermodynamic data (Lane and Ganguly, 1980; Wood and Yuen, 1983). Spinel with higher Cr/(Al + Cr) ratios (Cr#) can coexist with garnet at greater depths (e.g., O'Neill, 1981; Webb and Wood, 1986; Ganguly and Bhattacharya, 1987; Klemme, 2004).

Alpine-type peridotites and mantle xenoliths occasionally contain corona textures showing a garnet reaction rim developed around a spinel core, suggesting the preservation of garnet peridotite partially transformed from spinel peridotite (e.g., Obata, 1980; Obata and Morten, 1987; Ionov et al., 1993; Lee et al., 2001; Medaris et al., 2005). Some tectonic models and possible P–T paths inducing the transformation have been proposed based on

69 petrological studies (e.g., Obata and Morten, 1987; Brueckner and Medaris, 2000; Nimis
70 and Morten, 2000; Medaris et al., 2005). The corona texture may indicate that not only
71 textural equilibration, but also the garnet-forming reaction, were incomplete due to slow
72 reaction kinetics. If a metastable spinel core survives, it should place important constraints
73 on the P–T–t path. However, it has been difficult to interpret petrological observations from
74 a non-equilibrium point of view, because the mechanisms and kinetics of the reaction are
75 poorly known.

76 In this study, we conducted reaction experiments described in reaction (1) by
77 enclosing a spinel crystal in a two-pyroxene powder in the garnet peridotite stability field to
78 examine the mechanisms and kinetics of the spinel-to-garnet transformation in peridotite.
79 We also conducted the following reaction experiment by using a single-pyroxene powder
80 for comparison:

81 $$Opx + Spl = Grt + Ol \quad (2)$$

82 We experimentally reproduced the corona texture observed in natural rocks, and measured
83 the growth rate of the reaction rim. Future work on the metastability of a spinel core
84 rimmed by garnet in peridotite is discussed.

85

86 **EXPERIMENTAL METHODS**

87 A cubic-type multi-anvil apparatus (MAX-90) installed at Kyushu University,
88 Japan, was used for the high-P–T experiments. The truncated edge length of the anvils was
89 8 mm. The sample assembly consisted of a sintered pyrophyllite pressure medium, Mo
90 electrodes, and a stepped cylindrical graphite heater that also served as a sample capsule
91 (Fig. 2). The pressure was calibrated as a function of oil pressure on the basis of the
92 room-temperature transition of Bi(I) to Bi(II) (2.55 GPa) and the quartz–coesite transition

93 at 3.2 GPa and 1220°C (Bose and Ganguly, 1995). An additional pressure calibration was
94 conducted by using an in situ X-ray diffraction method using the same type of
95 high-pressure apparatus (MAX-80) at the synchrotron facility of the Photon Factory
96 (AR-NE5C), Tsukuba, Japan. Using NaCl as a pressure marker (Decker, 1971), we
97 confirmed that the pressure linearly increased with the applied load to ~3.5 GPa, and was
98 constant when heating to ~1000°C at a constant load. The temperature was measured using
99 a W25%Re–W3%Re thermocouple. The effect of pressure on the electromotive force of the
100 thermocouple was ignored. The temperature at the center of the sample capsule was higher
101 than that of the thermocouple by ~2% at 3.2 GPa and 1430°C on the basis of a
102 two-pyroxene thermobarometer (Ishibashi and Ikeda, 2005). The temperature gradient in
103 the sample capsule was estimated to be within ~1%–2% of the averaged temperature.
104 Crystals of orthopyroxene, clinopyroxene, spinel, and olivine without visible
105 inclusions were selected from a San Carlos mantle xenolith (spinel lherzolite) and were
106 used as the starting materials after ultrasonic cleaning in acetone. Chemical compositions of
107 the starting materials are listed in Table 1. Orthopyroxene and clinopyroxene were ground
108 to a powder (less than a few microns in size) and mixed at a molar ratio of 1:1. A single
109 spinel crystal was cut into a rectangular shape (dimensions, approximately 350–500 μm). In
110 most of the experiments, the single spinel crystal was embedded into the mixture of
111 powdered orthopyroxene and clinopyroxene in the sample capsule (Fig. 2). In some runs,
112 half of the spinel crystal was covered with olivine powder, and the other half was covered
113 with the powder mixture of the two pyroxenes. We also conducted an additional experiment
114 in which the spinel crystal was enclosed by powdered monomineralic orthopyroxene.
115 Samples were first compressed at room temperature and heated to the desired

116 temperature at constant oil pressure. The heating rate was controlled to ~100°C/min. All
117 reaction experiments were conducted in the garnet peridotite stability field at 3.2 GPa,
118 1020°C–1220°C, for 0.6–30 hours (Fig. 1). We used the spinel–garnet transition (i.e.,
119 garnet-in) boundary determined using natural mineral mixtures with similar Cr# in spinel of
120 ~0.08 (O'Hara et al., 1971) to our starting material, for which the pressure interval for the
121 coexisting field of spinel and garnet is estimated to be ~1 GPa (Webb and Wood, 1986). As
122 shown in Fig. 1, the present experimental conditions were thought to be beyond the
123 coexisting field (i.e., spinel-out) boundary. The sample was quenched to room temperature
124 by shutting off the electric power supply to the furnace at the high-pressure condition, and
125 the pressure was slowly released.

126 Recovered samples were cut parallel to the axial direction of the cylindrical heater
127 and were then polished to make thin sections. Reaction microstructures and chemical
128 compositions of existing phases were examined by a scanning electron microscope (SEM;
129 JEOL JSM-5800 and JSM-7001F) equipped with an energy dispersive X-ray spectrometer
130 (EDS). The SEM observations were conducted using one thin section from the central part
131 of the spinel crystal from each sample.

132 In some recovered samples, unpolarized infrared absorption spectra of the
133 polycrystalline pyroxene were obtained in air using a Fourier-transform infrared
134 spectrometer (FTIR; JASCO FTIR-4100 combined with an IRT-3000) and an InSb detector.
135 The samples were double-side-polished polycrystalline disks with thicknesses of 138–185
136 μm, dried at 120°C in an evacuated oven for >10 hours prior to measurements. The aperture
137 size was 100 × 100 μm. The water contents in the samples were estimated by integrating
138 the infrared absorption spectra based on the Paterson calibration (e.g., Paterson, 1982;
139 Keppler and Rauch, 2000; Mierdel et al., 2007). An anisotropy factor of 1/3 was used,

assuming a random orientation of the polycrystalline samples.

## RESULTS

Experimental conditions and results are summarized in Table 2. Microstructural observations of recovered samples reveal that the reaction rim of polycrystalline pyropic garnet formed between the single spinel crystal and the polycrystalline pyroxene (Fig. 3). The width of the garnet reaction rim increased with time and increasing temperature. During the initial stage of the reaction, garnets were formed preferentially along boundaries of pyroxene grains, resulting in some pyroxene grains being surrounded by garnet (Fig. 3a, b). These irregular garnet–pyroxene inter-phase boundaries became relatively planar with time and consisted in part of faceted garnet (Fig. 3c, d). On the other hand, the spinel–garnet inter-phase boundaries became irregular with time. In some regions, spinel inclusions were formed within the garnet reaction rim (Fig. 3c, d). The presence/absence of the irregular inter-phase boundary is summarized in Table 2. These morphological changes of the inter-phase boundary resulted in considerable variations in rim thickness.

Grains in the two-pyroxene aggregate matrix grew larger during annealing. No clear difference in grain size was observed in orthopyroxene versus clinopyroxene grains. Average grain sizes, as measured by the intercept method (Mendelson, 1969), are listed in Table 2. The grain size of pyroxene increased from ~2 to ~10 μm with increasing temperature and duration of heating; except during the early stages of the reaction, the grain size was smaller than the thickness of the garnet reaction rim.

In the experiment with the single spinel crystal enclosed by orthopyroxene powder (Run coro11), in addition to a garnet reaction rim, olivine grains with Mg/(Mg + Fe) ratios

(Mg#) of 0.90 also formed between the garnet reaction rim and the polycrystalline orthopyroxene (Fig. 3e). The olivine grains were less commonly observed in thin sections and were present in some domains without forming reaction rims. The amount of olivine was estimated to be ~10% of the garnet reaction rims; we did not observe any olivine grains in the experiments using the two-pyroxene powder.

Chemical compositions of garnet and pyroxene in recovered samples are summarized in Table 3. As we did not observe systematic changes in chemical compositions with run duration, the data were averaged over the different duration at each temperature. Garnets were pyropic at all temperatures. Both Mg# and Cr# values in garnet increased at high temperatures, while Ca contents remained nearly constant, except for a decrease in the experiment conducted using only orthopyroxene powder. No compositional variations in garnet across the rims were observed. On the other hand, the compositions of clinopyroxene became richer in Mg and poorer in Ca at high temperatures, while those of orthopyroxene showed fewer changes. The Tschermak component was nearly constant in both pyroxenes, although it should increase with temperature (e.g., Gasparik, 1984), which may suggest that the reaction rims of garnet and the surrounding pyroxenes did not reach complete chemical equilibrium.

The Mg# values of spinel increase towards the garnet reaction rim, which is visible as a bright-to-dark gradation in the backscatter electron (BSE) images, although the quantitative EDS measurements were difficult (Fig. 3). Enrichment of Cr in the spinel at the contact with garnet was also observed as white regions of ~1 μm wide in the BSE images (Fig. 3). Spinel grains enclosed in the newly formed garnet are typically rimmed by a zone of Cr-rich spinel (Fig. 3c–e). This possibly indicates that the Cr-component, which is less

compatible in garnet than in spinel, is preferentially retained in the retreating spinel. Similar enriched zone has been reported for the Ni component in olivine during the reaction rim growth of orthopyroxene by Milke et al. (2011).

The widths of the garnet reaction rim were measured at a point every ~10 μm in distance along the upper and lower parts of the spinel crystal. A total of ~30–80 measurements from each sample were averaged, and averaged values are listed in Table 2. The uncertainties become larger with time due to the development of the irregular spinel–garnet inter-phase boundaries. Figure 4 shows plots of the reaction rim width as a function of the square root of time. The rim width increased almost linearly with the square root of time, indicating diffusion-controlled growth of the garnet reaction rim. The kinetics of diffusion-controlled growth can be described by

$$\left[x(t)\right]^2 = kt \tag{3}$$

where x(t) is the rim width at time t and k is the rate constant (e.g., Fisher, 1978; Watson and Price, 2002). The value of k for a given temperature was obtained from the slope of a weighted least-squares linear regression line, as shown in Fig. 4 and summarized in Table 4. The temperature dependence of the rate constant k is expressed by

$$k = k_0 \exp\left(\frac{-H^*}{RT}\right) \tag{4}$$

where $k_0$ is the pre-exponential term, $H^*$ is the activation enthalpy, R is the gas constant, and T is absolute temperature. A weighted least-squares linear fitting of equation (4) to the present data yields $k_0 = 10^{-19.8 \pm 4.9}$ $m^2$ $s^{-1}$ and $H^* = 171 \pm 58$ kJ $mol^{-1}$, as shown in Fig. 5. The uncertainties are one standard deviation.

Unpolarized infrared absorption spectra from the polycrystalline pyroxene matrix

in recovered samples show a broad absorption band, from 2900 to 3700 $cm^{-1}$. Additional absorption peaks were observed at approximately 3400 and 3600 $cm^{-1}$ in samples treated at 1220°C. The water contents were estimated to be 40–120 wt. ppm $H_2O$ (Table 2). We observed no systematic changes in the water content with increasing temperature or duration of heating. Water content values were lower than those in natural pyroxenes from mantle xenoliths (200–500 wt. ppm $H_2O$; e.g., Bell and Rossman, 1992).

## DISCUSSION

### Mass balance calculations for the garnet-forming reaction between spinel and pyroxene

In the present study, garnet formed polycrystalline reaction rims between spinel and pyroxene in all experimental runs, while a smaller fraction of olivine (~10% of garnet) was observed only when the spinel crystal was surrounded by monomineralic orthopyroxene. The simplified model for reactions (1) and (2) can be written as follows on the basis of 12 oxygens:

$$(2 - 3y)/2\ [(1 - x)Mg_4Si_4O_{12} + xMg_2Al_4Si_2O_{12}] + 3y/2\ [(1 - x)Ca_2Mg_2Si_4O_{12} + xCa_2Al_4Si_2O_{12}] + (1 - 2x)/3\ Mg_3Al_6O_{12} = [(1 - y)Mg_3Al_2Si_3O_{12} + yCa_3Al_2Si_3O_{12}] + (1 - 2x)/3\ Mg_6Si_3O_{12} \quad (5)$$

where x is the Tschermak component in pyroxenes (in moles) and y is the grossular component in garnet (in moles). Assuming that the volume is approximately proportional to the amount of oxygen in each mineral, the reaction suggests that volumes of spinel consumed and olivine produced are the same, and that both decrease with an increase in the Tschermak component in pyroxenes. The volume ratio of olivine compared with garnet in products is estimated to be ~0.29, based on an x value of ~0.06–0.07 for pyroxene in the

232 reactants in our experiments. Thus, the reactions observed in our experiments seem to be
233 inconsistent with the ideal reaction (5).

234 To clarify the reactions that actually occurred, we performed mass-balance
235 calculations considering the various possible reactions (A–L), listed in Table 5. The
236 coefficients of each reaction were determined by a least squares method using the mineral
237 compositions listed in Tables 1 and 3, and summarized in Table 5. In the case of spinel
238 enclosed by orthopyroxene, the coefficients of spinel and olivine were not the same, and the
239 residual error was much larger than the errors of chemical analysis especially for Ca (A in
240 Table 5). Actually, the Ca content in the garnet reaction rim is high relative to that in the
241 starting orthopyroxene, implying that the diopside component in orthopyroxene (Di in Opx)
242 was preferentially consumed in the reaction. This is likely because a large amount of
243 pyroxene is present around the spinel crystal without direct involvement of the reaction.
244 When we adopted a composition of Di (in Opx) that was the same as that of orthopyroxene,
245 except with a Ca/(Mg + Fe + Ca) ratio of 0.5 (B in Table 5), the reaction was better defined
246 within the errors of chemical analysis (except for Fe), as follows:

247 $$0.83\ \mathrm{Opx} + 0.16\ \mathrm{Di\ in\ Opx} + 0.30\ \mathrm{Spl} = 1.00\ \mathrm{Grt} + 0.30\ \mathrm{Ol} \qquad (6)$$

248 The volumes of spinel and olivine in reaction (6) are equal, and are consistent with those
249 inferred from the principal reaction (5). However, the amount of olivine estimated from thin
250 sections of the recovered sample (~10%) is actually less than that inferred from reaction (6).
251 The SEM observations revealed that olivine grains do not form continuous reaction rims,
252 but are present as scattered domains, which indicates that nucleation of olivine is limited.
253 Thus, we may not have measured the actual olivine fraction accurately from thin sections of
254 the central part of the spinel crystal if olivine grains preferentially nucleated at the corners
255 of the crystal. Alternatively, the amount of olivine may decrease if Eskola (Es) components,

256 $(Ca,Mg,Fe)Al_2Si_4O_{12}$, in pyroxene are preferentially consumed by the reaction. By adopting
257 a Ca–Es component, which is well documented both in experiments (e.g., Zhao et al., 2011)
258 and natural mantle xenoliths (e.g., Smyth 1980), in reactant minerals, the reaction with 10%
259 olivine in products can be defined with only minor increases in the error as follows (C in
260 Table 5):

261 0.59 Opx + 0.09 Di in Opx + 0.15 Ca–Es + 0.26 Spl = 1.00 Grt + 0.10 Ol (7)

262 Although accurate quantification of the olivine fraction is difficult because of limited thin
263 section data, as mentioned above, the actual reaction occurring in the experiment involving
264 spinel enclosed by orthopyroxene may be intermediary between reactions (6) and (7).

265 Olivine was not observed in the experiments of spinel embedded in two-pyroxene
266 aggregates; however, the reaction without olivine in products should be excluded because
267 of large errors in the calculations compared to those of chemical analysis (D, E, and F in
268 Table 5). The errors decrease drastically if we adopt olivine in the products (G, H, and I in
269 Table 5); however, it is unlikely that the large amount of olivine inferred (~27%) was
270 missed in the thin sections. When we adopted a Ca–Es component in reactants, as discussed
271 above, the reaction with nearly zero olivine in the products is inferred to be a probable
272 solution (J, K, and L in Table 5). The stoichiometric coefficients averaged from all
273 temperatures are as follows (M in Table 5):

274 0.42 Opx + 0.17 Cpx + 0.20 Ca–Es + 0.23 Spl = 1.00 Grt + 0.02 Ol (8)

275 which is generally consistent with the absence of olivine in the SEM observations.

276 The residual errors in the proposed reactions (6)-(8) from the mass-balance
277 calculation are within those of chemical analysis except for Fe. The slightly larger errors in
278 Fe than those of chemical analysis may be due to ignoring the presence of ferric iron. The
279 reactions proposed here would change the diopside and Es components of residual

pyroxenes surrounding the spinel crystal; however, it was difficult to detect compositional changes in these components. For example, relatively Ca-rich garnet was produced in the experiment of spinel enclosed by orthopyroxene, even though changes in the diopside component in orthopyroxene during the reaction were undetectable (Tables 1 and 3), probably because the relatively large amount of pyroxene surrounding the spinel compensates for notable compositional changes.

Microstructural observations indicate that olivine did not form the reaction rim during the reaction between spinel and pyroxene, probably because nucleation of olivine is retarded as compared with the nucleation of garnet. The large barrier to olivine nucleation may have caused preferential dissolution of the Ca–Es component of pyroxene in our experiments, such that garnet was formed with a smaller olivine fraction than expected from principal reaction (5). These results are partly consistent with petrographic observations of natural peridotitic rocks, which show that the reaction rim is composed only of garnet, while newly formed olivine grains are generally difficult to distinguish from the original olivine (e.g., Obata and Morten, 1987; Chin et al., 2012). However, the preferential dissolution of the Ca–Es component that is inferred from our experiments may not occur in peridotitic rocks, where olivine grains are abundant and in close proximity to spinel. In this case, the nucleation of new grains is not necessarily required, as overgrowth of the original grains is possibly the dominant process of formation of metamorphic olivine.

In some runs at 1120°C and 1220°C, half of the spinel crystal was covered with olivine powder (Table1). In these runs, overgrowths of the original olivine grains may have occurred without preferential dissolution of the Ca–Es component (i.e., H and I in Table 5). The evolution of reaction rim widths appears to bear no relationship to the presence or absence of pre-existing olivine (Table 2 and Fig. 4), suggesting that preferential dissolution

had only a minor effect on growth kinetics.

## Mechanisms and kinetics of garnet rim growth

The present study examined a garnet reaction rim developed by diffusion-controlled growth. To identify the rate-controlling process for rim growth, it is necessary to investigate partial reactions occurring at the interface between newly formed garnet and reactants, namely spinel and pyroxenes; these reactions would reveal the nature of diffusive fluxes across the reaction rim, local volume changes at the reaction interface, and relationships between rim thickness and diffusivity of the rate-controlling element, as demonstrated for relatively simple reactions in previous studies (e.g., Abart et al., 2004, 2009; Götze et al., 2010; Gardés et al., 2011; Joachim et al., 2011). However, such a quantitative analysis of rim growth is difficult because of the complexities of the reactions, as mentioned above. Therefore, we provide below a qualitative discussion of the mechanisms and kinetics of the growth of garnet reaction rim.

The direction of rim growth is defined by differences in the diffusive fluxes of chemical components. The formation of garnet at the pyroxene–garnet interface requires the diffusion of $R_2O_3$ and MO components from spinel, where R and M represent trivalent and divalent cations, respectively, whereas the diffusion of $SiO_2$ and MO components from pyroxenes is necessary to form garnet at the spinel–garnet interface. If either of the $R_2O_3$ or $SiO_2$ components is immobile (i.e., $J_{MO}$, $J_{SiO2} >> J_{R2O3}$ or $J_{MO}$, $J_{R2O3} >> J_{SiO2}$), garnet predominantly grows toward the spinel or pyroxene side, respectively.

The growth direction is inferred from SEM observations of growth textures in the reaction rim. The presence of an irregular growth front at the garnet–pyroxene interface, preferential growth along two-pyroxene boundaries, and pyroxene inclusions in the reaction

328 rim (Fig. 3a, b) suggest that garnet grew into the pyroxene region. On the other hand, the
329 spinel–garnet interface also was irregular, and some spinel inclusions were present in the
330 reaction rim after longer durations of growth (Fig. 3c, d), which suggest that garnet also
331 grew into the spinel region. These growth textures suggest that the reaction rim grew in
332 both directions. Thus, we infer that both $SiO_2$ and $R_2O_3$ components are mobile and
333 contributed to rim growth.

334 Preferential growth of garnet along pyroxene grain boundaries was observed when
335 the reaction rim was relatively small, i.e., approximately the size of the pyroxene grains
336 (Fig. 3, Table 2), which suggests that chemical diffusion in two-pyroxene reactant regions
337 is the rate-controlling process at early stages. When the reaction rim becomes larger than
338 the size of the pyroxene grains, rim growth is controlled by diffusion through the garnet rim,
339 resulting in a flat pyroxene–garnet inter-phase boundary. It is noteworthy that, while spinel
340 is a single crystal, the spinel–garnet growth front also becomes irregular, incorporating
341 spinel inclusions into the reaction rim (Fig. 3c, d). An irregular spinel–garnet inter-phase
342 boundary has also been observed in natural peridotitic rocks (Obata and Morten, 1987).
343 Recently, similar features in a reaction interface were reported in ringwoodite growth
344 between majorite and ferropericlase (Dobson and Mariani, 2014). They suggested that the
345 irregular inter-phase boundary results from a double-diffusive instability. This explanation
346 would also be applicable to the garnet rim growth in our study. Enrichment of Cr in the
347 spinel at the contact with garnet (Fig. 3) reduces the chemical potential of spinel and
348 inhibits further growth of garnet, in which the reaction at the interface is rate limited by the
349 slow interdiffusion of the Cr-component in spinel (e.g., Suzuki et al., 2008). Alternatively,
350 the enrichment can be reduced by increasing the area of the interface at which the
351 Cr-component is released, resulting in the morphological instability in the reaction rim.

Although Dobson and Mariani (2014) discussed the measurements of the rim width more extensively by defining two thicknesses of intergrowth and rim growth regions, it may not be adequate for the case of our study because the irregular inter-phase boundary did not develop a clear intergrowth texture as observed in the previous study.

In spite of these morphological changes at the growth front, the time dependence of the averaged thickness of the reaction rim (Fig. 5) obeys a diffusion-controlled growth law (within errors). Previous studies have indicated that volume diffusion rates of divalent cations such as Fe, Mg, Mn, and Ca (e.g., Cygan and Lasaga, 1985; Schwandt et al., 1995; Ganguly et al., 1998) are more rapid than Si–Al inter-diffusion (van Mierlo et al., 2013; Nishi et al., 2013a) and Si self-diffusion (Shimojuku et al., 2014a) rates in garnet. The obtained k values (Table 4) are several orders of magnitude larger than the volume diffusion coefficients. The activation energies for the volume diffusion of Si–Al (van Mierlo et al., 2013; Nishi et al., 2013a) and Si (Shimojuku et al., 2014a) are much larger than those of garnet rim growth determined in this study; this may indicate that fast-path diffusion along grain boundaries in garnet contributes to garnet rim growth. However, the rate constant k in the diffusion-controlled growth model does not depend solely on the diffusion coefficient itself: it also depends on the thermodynamic driving force and molar volumes and chemical compositions of the reactant and product phases (e.g., Abart et al., 2009). Quantitative analysis of the kinematics of rim growth, which has not been conducted in this study, is required to compare the rate constant k with the diffusivity.

## IMPLICATIONS

A garnet corona around a spinel core has often been observed in garnet peridotite from alpine-type rocks and mantle xenoliths. This observation is generally interpreted as

376 evidence that the garnet peridotites were derived from spinel peridotite protoliths (e.g.,
377 Ionov et al., 1993; Brueckner and Medaris, 2000). The spinel–garnet transition boundary
378 broadens in natural peridotitic rocks containing Cr, as Cr-rich spinel can coexist with garnet
379 over a relatively wide pressure range (e.g., Ganguly and Bhattacharya, 1987). The Cr# of
380 spinel in contact with garnet coronas has been used as a geobarometer to estimate the
381 pressure required for the formation of garnet peridotite (e.g., Obata and Morten, 1987; Chin
382 et al., 2012), based on equilibrium phase relations (e.g., O'Neill, 1981).

383 Various P–T paths and tectonic settings for the spinel–garnet transformation in
384 peridotite have also been inferred from petrological studies (e.g., Obata, 1980; Obata and
385 Morten, 1987; Ionov et al., 1993; Nimis and Morten, 2000; Medaris et al., 2005; Kamei et
386 al., 2010; Chin et al., 2012). For example, Ionov et al. (1993) have examined mantle
387 xenoliths brought up from the spinel-garnet peridotite transitional zone in the
388 subcontinental lithospheric mantle and suggested that the observed reaction textures of
389 spinel relics rimmed by garnet were formed at ~1000°C by progressive increase in pressure
390 or decrease in temperature. On the other hand, Brueckner and Medaris (2000) classified
391 tectonic settings of various alpine-type garnet peridotites. Among them, in the case of the
392 ultra-high temperature (UHT) type subduction zone peridotite, garnet formed at the expense
393 of spinel as a result of cooling of the hot spinel peridotite from ~1200°C. The cooling rates
394 of some UHT garnet peridotites have been estimated to be $\sim 2\times10^{-2}$°C/yr in the Ronda
395 peridotite (Obata, 1980) and $\sim 5\times10^{-3}$°C/yr in the Mohelno peridotite of the Bohemian
396 Massif (e.g., Medaris *et al*., 2005). In other cases, the prograde type subduction zone
397 peridotite in their classification, relatively cold mantle fragments are transferred from the
398 mantle wedge into the subducting crust and carried to deeper levels. The Nonsberg

399 ultramafic body located at NE Italy, where garnet coronae with the width of about 300 μm
400 were observed (Obata and Morten, 1987), may be an example of this type, in which it has
401 been proposed that the garnet formed in the nearly isothermal path of the subduction stage
402 at ~850°C (Nimis and Morten, 2000).

403 In spite of these important petrological investigations on possible P-T paths
404 forming the garnet coronas, no detailed studies have been conducted on the stability of the
405 spinel core. If garnet reaction rim widths are kinetically controlled, the time scale of
406 formation can also be deduced. This study of the kinetics of rim growth may be a useful
407 first step for demonstrating the metastability of spinel cores observed in natural mantle
408 rocks. As a preliminary attempt to illustrate this, we calculated variations of the garnet rim
409 width based on our kinetic results along the proposed P-T paths with the estimated cooling
410 rates and typical mantle flow speeds of ~$10^{-2}$-$10^{-1}$ m/yr assuming that the growth rate
411 increases linearly with the excess pressure from the transition boundary. The result suggests
412 that the kinetics of the rim growth obtained in this study is rather fast in all tectonic settings
413 mentioned above. In this case, the spinel core rimmed by garnet found in garnet-bearing
414 peridotite does not mean that the transformation was kinetically inhibited, but the
415 transformation proceeded in equilibrium under the spinel-garnet peridotite transition field,
416 where spinel and garnet can thermodynamically coexist.

417 However, the true time scale could be different from the above calculation because
418 our experimental work is still in its infancy, and a reliable extrapolation of our kinetic data
419 to geological time scales is still not possible, for the following reasons. First, the kinetic
420 data were analyzed by applying a simple model that only accounts for parabolic growth
421 behavior, in which all potentially relevant kinetic processes are lumped into a single kinetic

parameter, the rate constant k. A quantitative analysis of the kinematics of reaction rim growth that incorporates multiple processes, as has been demonstrated in other reactions, is still needed (e.g., Abart et al., 2004, 2009; Götze et al., 2010; Gardés et al., 2011; Joachim et al., 2011). Second, to proceed further with the analysis, the reaction occurring at each interface must be clarified quantitatively, which was difficult in the present study because no olivine was newly formed using the two-pyroxene aggregate, probably on account of the preferential dissolution of the Ca–Es component. A more useful approach may be to include the olivine component in the starting material, as is the case in natural settings. Third, because we did not perform a step-wise quantitative analysis, the kinds of diffusion that control the kinetics of garnet rim growth have not been clarified. Recent experiments have demonstrated slow non-parabolic rim growth occurred by diffusion along the grain boundaries together with grain coarsening in reaction rims (Gardés et al., 2011; Nishi et al., 2013b; Shimojuku et al., 2014b). If rim growth kinetics were initially controlled by grain-boundary diffusion, then the growth rate may decrease on account of grain coarsening during rim growth, whereas in later stages the kinetics may be controlled by volume diffusion in reaction rims. This point should be taken into account when considering the relatively wide garnet rims that develop at geological timescales. Finally, we used powdered minerals (pyroxenes) as components of the starting materials, which are known to enhance reaction kinetics by incorporating absorbed water and strain energy (Rubie and Thompson, 1985). Although we did not observe any evidence that changes in water content and grain growth of pyroxenes influenced rim growth kinetics, it is desirable to use sintered polycrystalline samples instead of powdered samples.

## ACKNOWLEDGEMENTS

We thank M. Obata, T. Ikeda, M. Nishi, A. Toramaru, A. Shimojuku, N. Doi, and S Uehara for valuable discussions and technical assistance, and K. Shimada for help with the SEM observations. We acknowledge J. Ganguly and an anonymous reviewer for their constructive review. We are also grateful to A. Perchuk, M. Obata, Y. Liang, and R. Abart for their improvements of early versions of the manuscript. This work was supported by the Advanced Scientist Development Program of Kyushu University to M. N., and by JSPS KAKENHI Grant Nos 23654190 and 25247089 to T. Kubo. In situ X-ray diffraction experiments were conducted at PFAR-NE7 of the Photon Factory (project no. 2010G639).

## REFERENCES CITED

Abart, R., Kunze, K., Milke, R., Sperb, R., and Heinrich, W. (2004) Silicon and oxygen self diffusion in enstatite polycrystals: the Milke et al. (2001) rim growth experiments revisited. Contributions to Mineralogy and Petrology, 147, 633-636.

Abart, R., Petrishceva, E., Fisher, F.D., and Svoboda, J. (2009) Thermodynamic model for diffusion controlled reaction rim growth in a binary system: application to the forsterite-enstatite-quartz system. American Journal of Science, 309, 114 –131.

Bell, D.R., and Rossman, G.R. (1992) Water in earth's mantle: The role of nominally anhydrous minerals. Science, 255, 1391-1397.

Bose, K., and Ganguly, J. (1995) Quartz-coesite transition revisited: Reversal experimental determination at 500-1200°C and retrieved thermochemical properties. American Mineralogist, 80, 231-238.

469 Brueckner, H.K., and Medaris, L.G. (2000) A general model for the intrusion and evolution
470 of 'mantle' garnet peridotites in high-pressure and ultra-high-pressure
471 metamorphic terranes. Journal of Metamorphic Geology, 18, 123-133.
472 Chin, E.J., Lee, C.-T. A., Luffi, P., and Tice, M. (2012) Deep Lithospheric Thickening and
473 Refertilization beneath Continental Arcs: Case Study of the P, T and
474 Compositional Evolution of Peridotite Xenoliths from the Sierra Nevada,
475 California, Journal of Petrology, 53, 477-511.
476 Cygan, R.T., and Lasaga, A.C. (1985) Self-diffusion of magnesium in garnet at 750°C to
477 900°C. American Journal of Science, 285, 328-350.
478 Decker, D.L. (1971) High-Pressure Equation of State for NaCl, KCl, and CsCl. Journal of
479 Applied Physics, 42, 3239-3244.
480 Dobson, D.P. and Mariani, E. (2014) The kinetics of the reaction of majorite plus
481 ferropericlase to ringwoodite: Implications for mantle upwelling crossing the 660
482 km discontinuity, Earth and Planetary Science Letters, 408, 110-118.
483 Fisher, G.W. (1978) Rate laws in metamorphism. Geochimica et Cosmochimica Acta, 42,
484 1035-1050.
485 Ganguly, J., Cheng, W., and Chakraborty, S. (1998) Cation diffusion in aluminosilicate
486 garnets: Experimental determination in pyrope-almandine diffusion couples.
487 Contributions to Mineralogy and Petrology, 131, 171-180.
488 Ganguly, J. and Bhattacharya, P.K. (1987) Xenoliths in Proterozoic kimberlites from
489 southern India: petrology and geophysical implications, P.H. Nixon, Ed., Mantle
490 Xenoliths, p. 249–265, J. Wiley & Sons, New York.

Gardés, E., Wunder, B., Wirth, R., and Heinrich, W. (2011) Growth of multilayered polycrystalline reaction rims in the $MgO–SiO_2$ system, part I: experiments. Contributions to Mineralogy and Petrology, 161, 1-12.

Gasparik, T (1984) Two-pyroxene thermobarometry with new experimental data in the system $CaO\text{-}MgO\text{-}A1_2O_3\text{-}SiO_2$. Contributions to Mineralogy and Petrology, 87, 87-97.

Götze, L. C., Abart, R., Rybacki, E., Keller, L.M., Petrishcheva, E., and Dresen, G. (2010) Reaction rim growth in the System $MgO\text{-}Al_2O_3\text{-}SiO_2$ under uniaxial stress. Mineralogy and Petrology, 99, 263–277.

Ionov, D.A., Ashchepkov I.V., Stosch H.G., Witt-Eickschen, G., and Seck, H.A. (1993) Garnet peridotite xenoliths from the Vitim volcanic field, Baikal region: the natural of the garnet-spinel peridotite transition zone in the continental mantle. Journal of Petrology, 34, 1141-1175.

Ishibashi, H., and Ikeda, T. (2005) Evaluations and a revision of the pyroxene geothermometry (in Japanese with English abstract). Japanese Magazine of Mineralogical and Petrological Sciences, 34, 186-194.

Joachim, B., Gardés, E, Abart, R., and Heinrich, W. (2011) Experimental growth of åkermanite reaction rims between wollastonite and monticellite: evidence for volume diffusion control. Contributions to Mineralogy and Petrology, 161, 389-399.

Kamei, A., Obata, M., Michibayashi, K., Svojtka, M., and Hirajima, T. (2010) Two contrasting fabric patterns of olivine observed in garnet and spinel peridotite from a mantle-derived ultramafic mass enclosed in felsic granulite, the Moldanubian

514 Zone, Czech Republic. Journal of Petrology, 51, 101-123.
515 Keppler, H., and Rauch, M. (2000) Water solubility in nominally anhydrous minerals
516 measured by FTIR and $^{1}$H MAS NMR: the effect of sample preparation. Physics
517 and Chemistry of Minerals, 27, 371-376.
518 Klemme, S., and O'Neill, H.S. (2000) The near solidus transition from garnet lherzolite to
519 spinel lherzolite. Contributions to Mineralogy and Petrology, 138, 237-248.
520 Klemme, S. (2004) The influence of Cr on the garnet-spinel transition in the Earth's
521 mantle: experiments in the system $MgO$-$Cr_2O_3$-$SiO_2$ and thermodynamic
522 modelling. Lithos, 77, 639-646.
523 Kushiro, I., and Yoder, H.S. (1966) Anorthite-forsterite and anorthite-enstatite reactions and
524 their bearing on the basalt-eclogite transformation. Journal of Petrology, 7,
525 337-362.
526 Lane, D.L. and Ganguly, J. (1980) $Al_2O_3$ solubility in orthopyroxene in the system
527 $MgO$-$Al_2O_3$-$SiO_2$: A reevaluation, and mantle geotherm. Journal of Geophysical
528 Research,85, 6963-6972.
529 Lee, C.-T., Rudnick, R.L., and Brimhall, G.H., Jr (2001) Deep lithospheric dynamics
530 beneath the Sierra Nevada during the Mesozoic and Cenozoic as inferred from
531 xenolith petrology. Geochemistry Geophysics Geosystems, 2, 1-27.
532 Medaris, G., Wang, H., Jelínek, E., Mihaljevič, M., and Jakeš, P. (2005) Characteristics and
533 origins of diverse Variscan peridotites in the Gföhl Nappe, Bohemian Massif,
534 Czech Republic. Lithos, 82, 1-23.
535 Mendelson, M.L. (1969) Average grain size in polycrystalline ceramics. Journal of the
536 American Ceramic Society, 52, 443-446.
537 Mierdel, K., Keppler, H., Smyth, J.R., and Langenhorst, H. (2007) Water solubility in

alminous orthopyroxene and the origin of earth's asthenosphere. Science, 315, 364-368.

Milholland, C.S., and Presnall, D. (1998) Liquidus phase relations in the $CaO$-$MgO$-$Al_2O_3$-$SiO_2$ system at 3.0 GPa: The aluminous pyroxene thermal divide and high-pressure fractionation of picritic and komatiitic magmas. Journal of Petrology, 39, 3-27.

Milke, R., Abart, R., Keller, L., and Rhede, D. (2011) The behavior of Mg, Fe, and Ni during the replacement of olivine by orthopyroxene: experiments relevant to mantle metasomatism. Mineralogy and Petrology, 103, 1-8.

Nimis, P., and Morten, L. (2000) P-T evolusion of 'cyustal' garnet peridotites and included pyroxnenites from Nonsberg area (upper Austroalpine), NE Italy: from the wedge of the slab. Journal of Geodynamics, 30, 93-115.

Nishi, M., Kubo, T., Ohfuji, H., Kato, T., Nishihara, Y., and Irifune, T. (2013a) Slow Si-Al interdiffusion in garnet and stagnation of subducting slabs. Earth and Planetary Science Letters, 361, 44-49.

Nishi, M., Nishihara, Y., and Irifune, T. (2013b) Growth kinetics of $MgSiO_3$ perovskite reaction rim between stishovite and periclase up to 50 GPa and its implication for grain boundary diffusivity in the lower mantle. Earth and Planetary Science Letters, 377-378, 191-198.

Obata, M. (1980) The Ronda peridotite: garnet, spinel and plagioclase lherzolite facies and the P–T trajectories of a high temperature mantle intrusion. Journal of Petrology, 21, 533–572.

Obata, M., and Morten, L. (1987) Transformation of spinel lherzolite to garnet lherzolite in ultramafic lenses of the Austridic crystalline complex, northern Italy. Journal of

562 Petrology, 28, 599-623.
563 O'Hara, M.J., Richardson, S. W., and Willson G. (1971) Garnet-peridotite stability and
564 occurrence in crust and mantle. Contributions to Mineralogy and Petrology, 32,
565 48-68.
566 O'Neill, H.St.C. (1981) The transition between spinel lherzolite and garnet lherzolite, and
567 its use as a geobarometer. Contributions to Mineralogy and Petrology, 77,
568 185-194.
569 Paterson, M.S. (1982) The determination of hydroxyl by infrared absorption in quartz,
570 silicate glasses and similar materials. Bulletin of Mineralogy, 105, 20-29.
571 Rubie, D.C., and Thompson, A.B. (1985) Kinetics of metamorphic reactions at elevated
572 temperaturesand pressures: An appraisal of available experimental data, A.B.
573 Thompson and D.C. Rubie, Eds., Metamorphic Reactions: Kinetics, Textures and
574 Deformation, p. 27-79, Springer-Verlag, New York.
575 Schwandt, C.S., Cygan, R.T., and Westrich, H.R. (1995) Mg self-diffusion in pyrope garnet.
576 American Mineralogist, 80, 483-490.
577 Shimojuku, A., Kubo, T., Kato, T., Yoshino, T., Nishi, M., Nakamura, T., Okazaki, R., and
578 Kakazu, Y. (2014a) Effects of pressure and temperature on the silicon diffusivity
579 of pyrope-rich garnet, Physics of the Earth and Planetary Interiors, 226, 28-38.
580 Shimojuku, A., Boujibar, A., Yamazaki, D., Yoshino, T., Tomioka, N., and Xu, J. (2014b)
581 Growth of ringwoodite reaction rims from $MgSiO_3$ perovskite and periclase at
582 22.5 GPa and 1,800 °C, Physics and Chemistry of Minerals 41, 555-567.
583 Suzuki, A.M., Yasuda, A., and Ozawa, K. (2008) Cr and Al diffusion in chromite spinel:
584 experimental determination and its implication for diffusion creep, Physics and
585 Chemistry of Minerals, 35, 433-445.

586 Smyth, J.R. (1980) Cation vacancies and the crystal-chemistry of breakdown reactions in
587 kimberlitic omphacites. American Mineralogist, 65, 1185–1191.
588 van Mierlo, W.L., Langenhorst, F., Frost, D.J., and Rubie, D.C. (2013) Stagnation of
589 subducting slabs in the transition zone due to slow diffusion majoritic garnet.
590 Nature Geoscience, 6, 400-403.
591 Walter, M., Katsura, T., Kubo, A., Shinmei, T., Nishikawa, O., Ito, E., Lesher, C., and
592 Funakoshi, K. (2002) Spinel-garnet lherzolite transition in the system
593 $CaO$-$MgO$-$Al_2O_3$-$SiO_2$ revisited: An in situ X-ray study. Geochimica et
594 Cosmochimica Acta, 66, 2109-2121.
595 Watson, E. B., and Price, J.D. (2002) Kinetics of the reaction $MgO + Al_2O_3 \rightarrow MgAl_2O_4$
596 and Al-Mg interdiffusion in spinel at 1200 to 2000°C and 1.0 to 4.0 GPa.
597 Geochimica et Cosmochimica Acta, 66, 2123-2138.
598 Webb, S.A.C., and Wood, B.J. (1986) Spinel-pyroxene-garnet relationships and their
599 dependence on Cr/Al ratio. Contributions to Mineralogy and Petrology, 92,
600 471-480.
601 Wood, B.J., and Yuen, D.A. (1983) The role of lithospheric phase transitions on seafloor
602 flattening at old ages. Earth and Planetary Science Letters, 66, 303-314.
603 Zhao, S., Nee, P., Green, H.W., and Dobrzhinetskaya, L.F. (2011) Ca-Eskola component in
604 clinopyroxene: Experimental studies at high pressures and high temperatures in
605 multianvil apparatus. Earth and Planetary Science Letters, 307, 517-524.
606
607
608 **Figure captions**

**FIGURE 1.** Pressure–temperature diagram showing the boundary of the spinel–garnet transformation in peridotite. The garnet-in boundary (solid curve) was determined using natural mineral mixtures, with a Cr/(Al + Cr) ratio (Cr#) in spinel of ~0.08 (O'Hara et al., 1971). The spinel-out boundary (dotted curve) assumes a pressure of ~1 GPa for the coexisting field (Webb and Wood, 1986). Experimental conditions of the present study are shown by solid circles.

**FIGURE 2.** Cross-section of the sample assembly.

**FIGURE 3.** Backscatter electron (BSE) images of recovered samples showing reaction textures. Spl: spinel; Grt: garnet; Opx: orthopyroxene; Cpx: clinopyroxene; Ol: olivine. The garnet reaction rim is formed between polycrystalline pyroxene and a single spinel crystal. Chromium-enriched spinel (Cr-rich Spl) in contact with garnet is observed as white regions. (a) Run coro08 (1020°C, for 10 hours), (b) Run coro04 (1170°C, for 2 hours), (c) Run coro06 (1220°C, for 10 hours), (d) Run coro17 (1220°C, for 30 hours), and (e) Run coro11 (1220°C, for 10 hours; with monomineralic orthopyroxene).

**FIGURE 4.** Plots of the width of the garnet reaction rim as a function of the square root of time. Results of the linear weighted least-squares fitting of equation (3) to the data are shown by straight lines.

**FIGURE 5.** Temperature dependence of the rate constant k. Result of the linear weighted least-squares fitting of equation (4) to the data is shown by a straight line.

Table 1. Chemical compositions of minerals from San Carlos mantle xenolith used in this study. Values in parentheses represent one standard deviation in the last digit evaluated by multiple analyses. Abbreviations are orthopyroxene (Opx), clinopyroxene (Cpx), spinel (Spl), olivine (Ol).

| | Opx | Cpx | Spl | Ol |
|---|---|---|---|---|
| $SiO_2$ (wt.%) | 55.41(97) | 53.00(76) | 0.00(0) | 40.12(34) |
| $Al_2O_3$ | 2.75(12) | 4.25(17) | 57.75(0) | 0.00(0) |
| $Cr_2O_3$ | 0.67(8) | 1.58(11) | 7.78(82) | 0.00(0) |
| FeO | 5.78(14) | 2.62(9) | 10.87(35) | 0.43(32) |
| $Ni_2O_5$ | 0.00(0) | 0.00(0) | 0.00(0) | 0.41(4) |
| MgO | 33.36(53) | 16.11(38) | 20.78(64) | 49.00(49) |
| CaO | 0.87(6) | 20.29(34) | 0.00(0) | 0.00(0) |
| $Na_2O$ | 0.00(0) | 1.48(99) | 0.00(0) | 0.00(0) |
| Total | 98.84(168) | 99.34(132) | 98.09(100) | 98.96(61) |
| Cations per 12 oxygens | | | | |
| Si | 3.880(0) | 3.859(5) | 0.000(0) | 2.982(8) |
| Al | 0.236(3) | 0.360(5) | 5.394(75) | 0.000(0) |
| Cr | 0.040(0) | 0.085(4) | 0.488(59) | 0.000(0) |
| Fe | 0.336(5) | 0.160(0) | 0.722(34) | 0.585(23) |
| Ni | 0.000(0) | 0.000(0) | 0.000(0) | 0.025(5) |
| Mg | 3.484(3) | 1.749(7) | 2.454(24) | 5.428(23) |
| Ca | 0.076(3) | 1.581(7) | 0.000(0) | 0.000(0) |
| Na | 0.000(0) | 0.205(4) | 0.000(0) | 0.000(0) |
| Sum | 8.052(3) | 8.013(5) | 9.059(9) | 9.018(8) |

Table 2. Experimental conditions and results. All experiments were carried out at 3.2 GPa. Spinel single crystal was enclosed by the two-pyroxene powder except for Run coro11. The reaction rim of pyropic garnet was formed in all runs. Values in parentheses represent the uncertainties.

| Run no. | Temp. (°C) | Time (h) | Reaction rim width (μm) | Pyroxene grain size (μm) | Irregular inter-phase boundary | Water content[a] (wt.ppm) |
|---|---|---|---|---|---|---|
| coro08 | 1020 | 10 | 2.2 (1.1) | 3.1 | Px-Grt | - |
| coro07 | 1020 | 20 | 4.0 (1.6) | 4.1 | Px-Grt | 90 (10) |
| coro15[b] | 1120 | 0.6 | 2.0 (0.7) | 1.4 | Px-Grt | - |
| coro16[b] | 1120 | 5 | 3.5 (0.7) | 3.3 | Px-Grt, Spl-Grt | - |
| coro09 | 1120[c] | 10 | 7.2 (1.5) | 6.0 | Spl-Grt | 50 (10) |
| coro13 | 1120 | 20 | 9.0 (1.8) | 6.7 | Spl-Grt | 40 (10) |
| coro18[b] | 1120 | 30 | 13.6 (1.8) | 7.0 | Spl-Grt | - |
| coro04 | 1170 | 2 | 4.2 (2.0) | 4.1 | Px-Grt | - |
| coro03 | 1220[c] | 1 | 2.6 (1.2) | 2.7 | Px-Grt | - |
| coro02 | 1220 | 5 | 6.8 (2.5) | 5.9 | Spl-Grt | 120 (30) |
| coro06 | 1220 | 10 | 8.5 (1.9) | 6.9 | Spl-Grt | 70 (20) |
| coro11[d] | 1220 | 10 | 6.9 (2.4) | 9.5 | Spl-Grt | 100 (20) |
| coro05 | 1220 | 20 | 13.6 (5.3) | 8.5 | Spl-Grt | 120 (50) |
| coro17[b] | 1220 | 30 | 15.5 (4.1) | 10.0 | Spl-Grt | - |

[a]Water contents in the pyroxene regions were measured in some samples.

[b]Half of the spinel crystal was covered with olivine powder instead of the two-pyroxene pyroxene powder.

[c]Temperature was estimated from the power supply.

[d]Spinel was enclosed by the orthopyroxene powder, and olivine grains were formed in addition to the garnet reaction rim.

Table 3. Chemical compositions of constituent minerals in recovered samples averaged over the different duration at each temperature. Values in parentheses represent one standard deviation in the last digit evaluated. Abbreviations are orthopyroxene (Opx), clinopyroxene (Cpx), garnet (Grt), spinel (Spl), olivine (Ol).

| | 1220°C | | | 1120°C | | |
|---|---|---|---|---|---|---|
| | Opx | Cpx | Grt | Opx | Cpx | Grt |
| $SiO_2$ | 55.45(117) | 53.23(125) | 42.12(220) | 55.59(199) | 54.18(91) | 41.79(75) |
| $Al_2O_3$ | 2.96(46) | 3.65(92) | 20.72(308) | 3.42(244) | 2.61(44) | 21.59(48) |
| $Cr_2O_3$ | 0.75(12) | 1.21(19) | 2.72(63) | 0.75(24) | 1.18(28) | 2.71(57) |
| FeO | 5.25(38) | 3.07(25) | 6.36(75) | 5.50(36) | 2.72(16) | 7.05(52) |
| MgO | 32.96(181) | 19.12(149) | 20.62(79) | 33.20(185) | 18.63(92) | 20.34(69) |
| CaO | 1.84(172) | 18.13(161) | 6.67(209) | 1.50(90) | 19.62(103) | 6.31(54) |
| $Na_2O$ | 0.00(0) | 0.57(37) | 0.00(0) | 0.00(0) | 0.88(39) | 0.00(0) |
| Total | 99.20(164) | 98.97(205) | 99.23(155) | 99.96(104) | 99.80(117) | 99.79(137) |
| Cations per 12 oxygens | | | | | | |
| Si | 3.86(3) | 3.86(4) | 3.02(15) | 3.84(12) | 3.91(2) | 2.99(3) |
| Al | 0.24(4) | 0.31(8) | 1.75(26) | 0.28(20) | 0.22(3) | 1.82(4) |
| Cr | 0.04(1) | 0.07(1) | 0.15(4) | 0.04(1) | 0.07(2) | 0.15(3) |
| Fe | 0.31(2) | 0.19(2) | 0.38(5) | 0.32(2) | 0.16(1) | 0.42(3) |
| Mg | 3.41(14) | 2.07(15) | 2.20(7) | 3.41(17) | 2.01(8) | 2.17(6) |
| Ca | 0.14(14) | 1.41(13) | 0.51(17) | 0.11(7) | 1.51(8) | 0.48(4) |
| Na | 0.00(0) | 0.08(5) | 0.00(0) | 0.00(0) | 0.12(5) | 0.00(0) |
| Sum | 8.00(1) | 7.99(4) | 8.03(1) | 8.00(2) | 8.01(3) | 8.03(1) |

| | 1020°C | | | 1220°C (Sp enclosed by Opx) | | |
|---|---|---|---|---|---|---|
| | Opx | Cpx | Grt | Opx | Grt | Ol |
| $SiO_2$ | 55.67(137) | 53.58(97) | 42.04(135) | 54.31(32) | 40.02(94) | 39.89(21) |
| $Al_2O_3$ | 3.05(170) | 3.34(65) | 21.72(138) | 3.20(10) | 21.51(39) | 0.00(0) |
| $Cr_2O_3$ | 0.72(27) | 1.31(21) | 2.30(36) | 0.63(10) | 3.32(51) | 0.31(0) |
| FeO | 5.63(41) | 2.82(21) | 7.70(34) | 5.48(26) | 6.69(12) | 9.28(9) |
| MgO | 32.55(132) | 18.00(135) | 20.30(56) | 33.18(24) | 21.12(29) | 47.34(59) |

| | | | | | | |
|---|---|---|---|---|---|---|
| CaO | 2.14(116) | 19.49(129) | 6.48(64) | 1.11(6) | 4.60(26) | 0.28(0) |
| $Na_2O$ | 0.00(0) | 0.68(49) | 0.00(0) | 0.00(0) | 0.00(0) | 0.00(0) |
| Total | 99.76(107) | 99.22(132) | 100.54(225) | 97.91(18) | 97.27(24) | 96.79(89) |
| Cations per 12 oxygens | | | | | | |
| Si | 3.86(9) | 3.89(4) | 2.99(6) | 3.83(2) | 2.93(6) | 3.03(4) |
| Al | 0.25(14) | 0.29(6) | 1.82(9) | 0.27(1) | 1.86(4) | 0.00(0) |
| Cr | 0.04(2) | 0.07(1) | 0.13(2) | 0.04(1) | 0.19(3) | 0.02(0) |
| Fe | 0.33(2) | 0.17(1) | 0.46(2) | 0.32(2) | 0.41(1) | 0.59(0) |
| Mg | 3.36(14) | 1.95(12) | 2.15(7) | 3.49(3) | 2.30(3) | 5.35(4) |
| Ca | 0.16(9) | 1.52(12) | 0.49(5) | 0.08(1) | 0.36(2) | 0.02(0) |
| Na | 0.00(0) | 0.10(7) | 0.00(0) | 0.00(0) | 0.00(0) | 0.00(0) |
| Sum | 8.00(3) | 7.98(3) | 8.04(3) | 8.02(2) | 8.05(2) | 8.97(3) |

This is a preprint, the final version is subject to change, of the American Mineralogist (MSA)
Cite as Authors (Year) Title. American Mineralogist, in press.
(DOI will not work until issue is live.) DOI: http://dx.doi.org/10.2138/am-2016-5586

Table 4: Estimated values of the rate constant k.

| Temperature (°C) | $k$ ($m^2/s$) |
|---|---|
| 1220 | $2.2\ (1.6\sim2.8) \times 10^{-15}$ |
| 1120 | $1.2\ (1.0\sim1.4) \times 10^{-15}$ |
| 1020 | $1.7\ (0.8\sim3.0) \times 10^{-16}$ |

This is a preprint, the final version is subject to change, of the American Mineralogist (MSA)
Cite as Authors (Year) Title. American Mineralogist, in press.
(DOI will not work until issue is live.) DOI: http://dx.doi.org/10.2138/am-2016-5586

*Table 5: Summary for the mass-balance calculation of the garnet-forming reaction between spinel and pyroxene by the least square method. Mineral compositions listed in Table 1 and 3 were used in the calculation for reactants and products, respectively.*

| Reaction | Spl enclosed by Opx | | | Spl enclosed by 2Px | | | | | | | | | | |
|---|---|---|---|---|---|---|---|---|---|---|---|---|---|---|
| | | Di in | Ca-Es Di in | no Ol in product | | | Ol in product | | | Ca-Es in reactant, Ol in product | | | | |
| Temp. | 1220°C | 1220°C | 1220°C | 1220°C | 1120°C | 1020°C | 1220°C | 1120°C | 1020°C | 1220°C | 1120°C | 1020°C | average | s.d. |
| | A | B | C | D | E | F | G | H | I | J | K | L | M | |
| Stoichiometric coefficients (O=12, Grt=1) | | | | | | | | | | | | | | |
| (Reactants) | | | | | | | | | | | | | | |
| Opx | 1.070 | 0.831 | 0.589 | 0.275 | 0.267 | 0.261 | 0.690 | 0.720 | 0.710 | 0.416 | 0.454 | 0.387 | 0.419 | 0.034 |
| Di in Opx[a] | - | 0.156 | 0.089 | - | - | - | - | - | - | - | - | - | - | - |
| Cpx | - | - | - | 0.458 | 0.453 | 0.459 | 0.291 | 0.270 | 0.278 | 0.183 | 0.166 | 0.151 | 0.167 | 0.016 |
| Ca-Es[b] | - | - | 0.149 | - | - | - | - | - | - | 0.190 | 0.185 | 0.225 | 0.200 | 0.022 |
| Spl | 0.299 | 0.302 | 0.261 | 0.265 | 0.277 | 0.276 | 0.276 | 0.288 | 0.288 | 0.225 | 0.239 | 0.228 | 0.231 | 0.007 |
| (Products) | | | | | | | | | | | | | | |
| Grt[c] | 1.000 | 1.000 | 1.000 | 1.000 | 1.000 | 1.000 | 1.000 | 1.000 | 1.000 | 1.000 | 1.000 | 1.000 | 1.000 | - |
| Ol | 0.403 | 0.300 | 0.100[c] | - | - | - | 0.259 | 0.283 | 0.280 | 0.021 | 0.052 | 0.000 | 0.024 | 0.026 |
| Residual error (products-reactants, O=12) | | | | | | | | | | | | | | |
| Si | 0.007 | -0.002 | -0.005 | -0.185 | -0.204 | -0.203 | -0.002 | -0.003 | -0.005 | -0.002 | -0.003 | -0.005 | | |
| Al | 0.008 | 0.006 | 0.007 | -0.094 | -0.101 | -0.099 | 0.002 | 0.004 | 0.005 | 0.006 | 0.008 | 0.010 | | |
| Cr | -0.013 | -0.012 | -0.041 | 0.026 | 0.033 | 0.054 | 0.029 | 0.036 | 0.057 | -0.011 | -0.003 | 0.010 | | |
| Fe | -0.072 | -0.063 | -0.068 | -0.024 | -0.060 | -0.097 | -0.057 | -0.095 | -0.132 | -0.062 | -0.101 | -0.138 | | |
| Mg | 0.005 | 0.008 | 0.012 | 0.209 | 0.233 | 0.236 | 0.007 | 0.012 | 0.017 | 0.008 | 0.013 | 0.018 | | |
| Ca | -0.287 | 0.002 | 0.005 | 0.230 | 0.254 | 0.252 | -0.007 | -0.006 | -0.006 | -0.003 | -0.002 | -0.001 | | |
| Na | 0.000 | 0.000 | 0.000 | 0.094 | 0.093 | 0.094 | 0.060 | 0.055 | 0.057 | 0.038 | 0.034 | 0.031 | | |
| Error sum of squares | 0.088 | 0.004 | 0.006 | 0.150 | 0.184 | 0.192 | 0.008 | 0.014 | 0.024 | 0.006 | 0.012 | 0.021 | | |

[a]Diopside component in Opx that has the same composition as Opx except for Ca/(Mg+Fe+Ca) of 0.5.

[b]Ca-Eskola component in pyroxenes ($CaAl_2Si_4O_{12}$).

[c]Stoichiometric coefficient was fixed in the calculation.

Figure 1

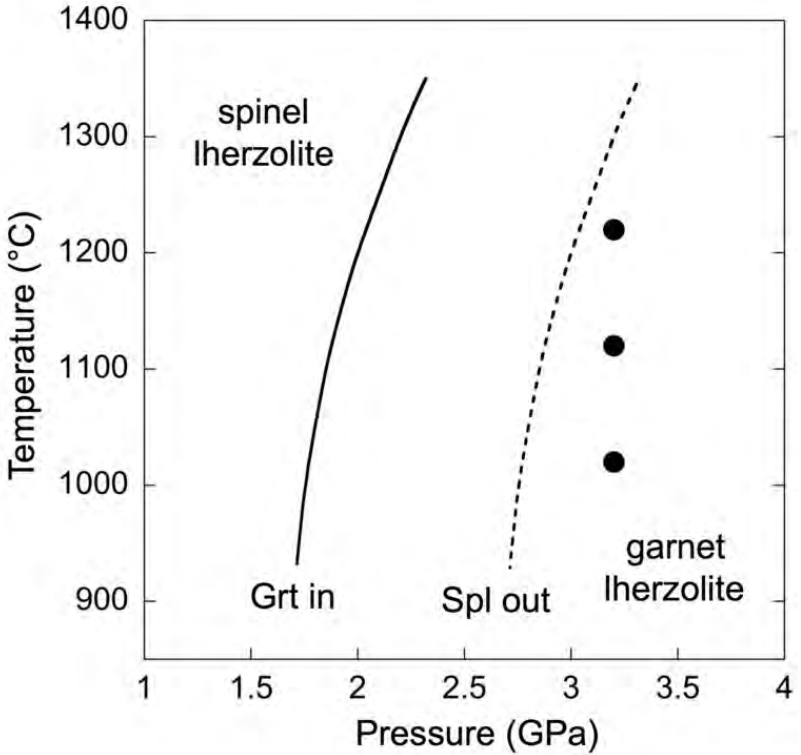
1400
1300
1200
1100
1000
900
Temperature (°C)
spinel
lherzolite
garnet
lherzolite
Grt in
Spl out
1
1.5
2
2.5
3
3.5
4
Pressure (GPa)

Figure 2

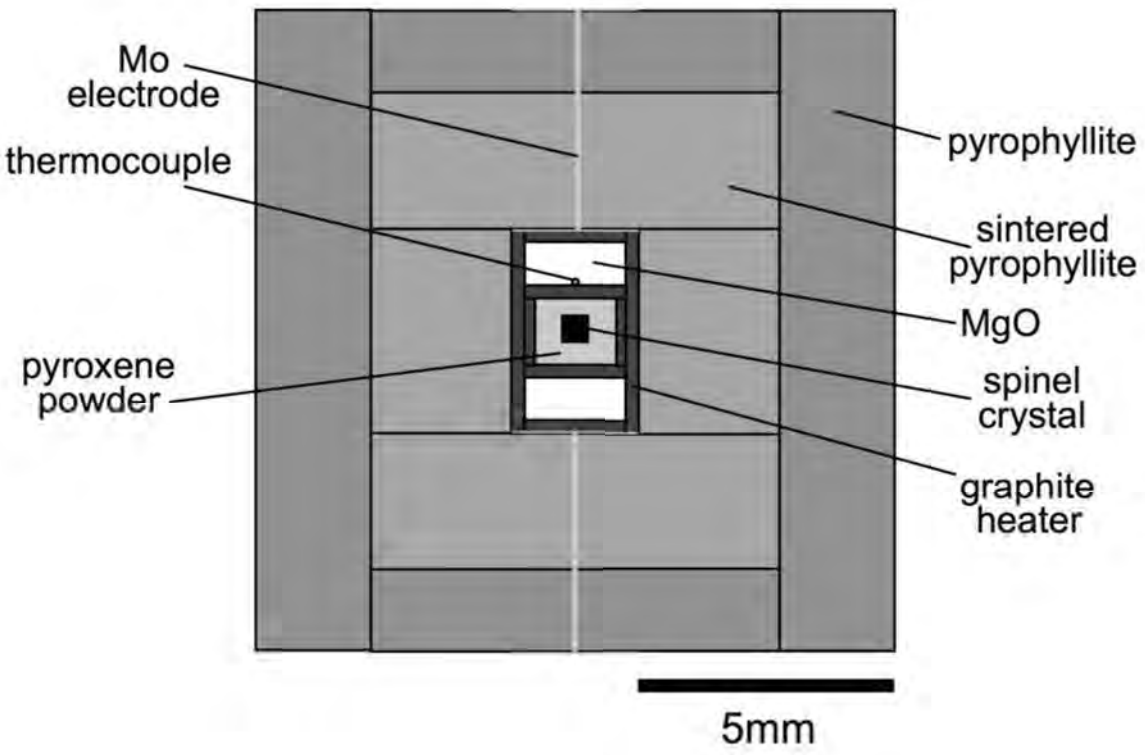
Mo
electrode
thermocouple
pyroxene
powder
pyrophyllite
sintered
pyrophyllite
MgO
spinel
crystal
graphite
heater
5mm

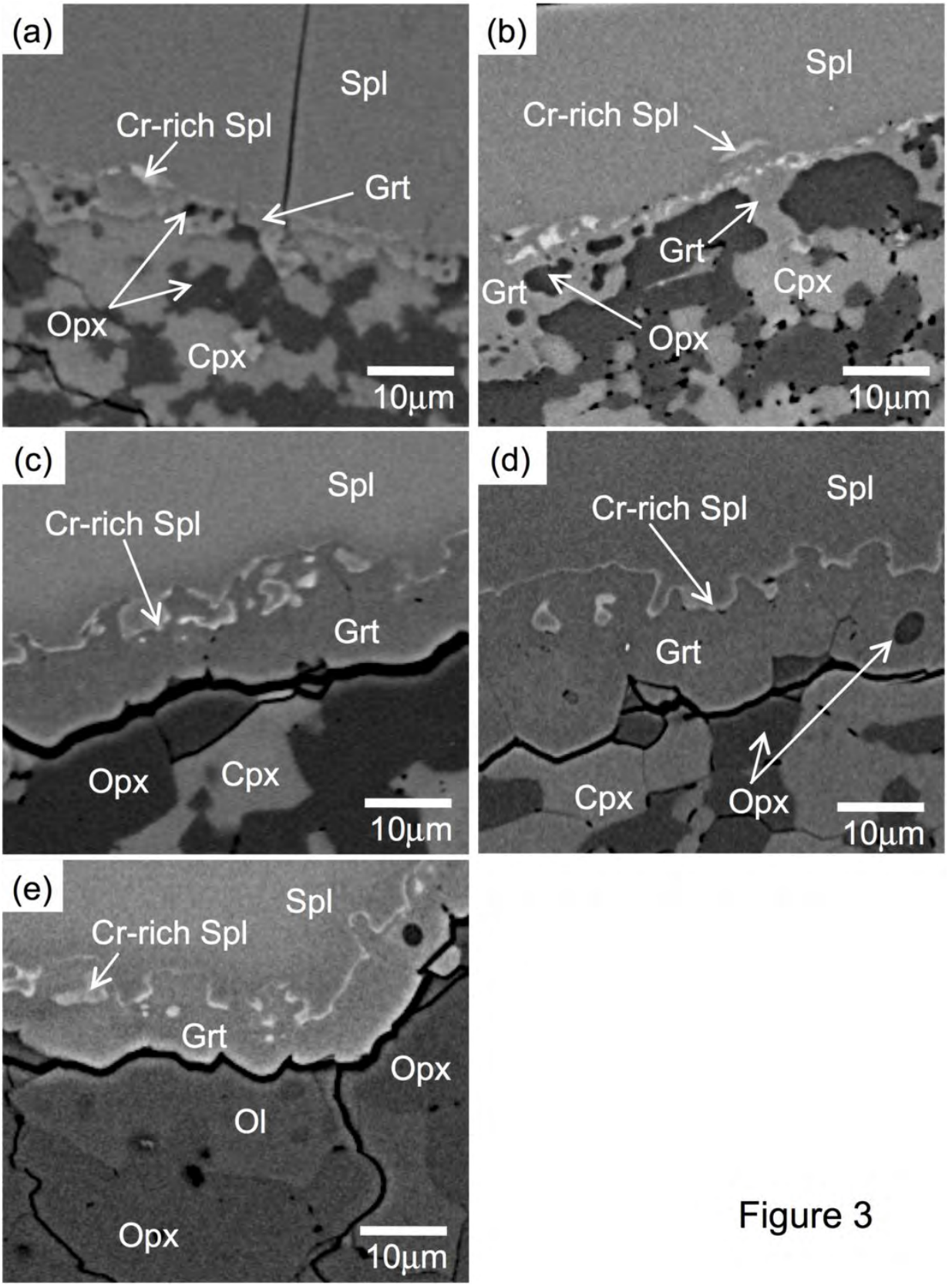
(a)
Spl
Cr-rich Spl
Grt
Opx
Cpx
10μm
(b)
Spl
Cr-rich Spl
Grt
Grt
Cpx
Opx
10μm
(c)
Spl
Cr-rich Spl
Grt
Opx
Cpx
10μm
(d)
Spl
Cr-rich Spl
Grt
Cpx
Opx
10μm
(e)
Spl
Cr-rich Spl
Grt
Opx
Ol
Opx
10μm

Figure 3

Figure 4

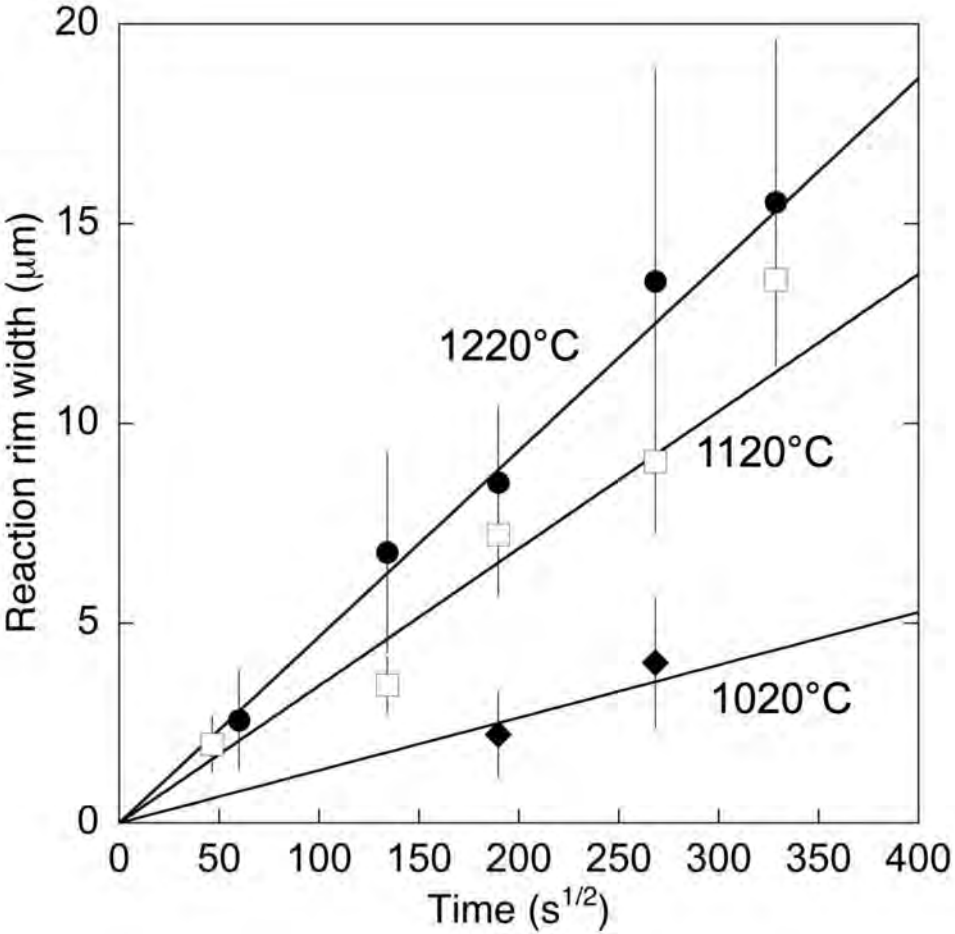
20
15
10
5
0
Reaction rim width (μm)
1220°C
1120°C
1020°C
0
50
100
150
200
250
300
350
400
Time (s^1/2)

Figure 5